Hindawi
Journal of Advanced Transportation
Volume 2020, Article ID 7943739, 15 pages
https://doi.org/10.1155/2020/7943739

Research Article

Study on the Influence of Road Geometry on Vehicle Lateral Instability

Yanna Yin,[1] **Huiying Wen**,[1] **Lu Sun**,[1,2] **and Wei Hou**[3,4]

[1]*South China University of Technology, School of Civil Engineering and Transportation, No. 381 Wushan Road Tianhe District, Guangzhou 510641, China*
[2]*Department of Civil and Environmental Engineering, University of Maryland, College Park, MD 20742, USA*
[3]*Qilu Transportation Development Group Co., Ltd., Lixia District, Jinan, China*
[4]*Shangdong Binlai Freeway Ltd., Zibo, Shandong Province, China*

Correspondence should be addressed to Lu Sun; workingworking123@163.com

Received 17 November 2019; Revised 24 June 2020; Accepted 17 September 2020; Published 7 October 2020

Academic Editor: Maria Castro

According to the accident analysis of vehicles in the curve, the skidding, rollover, and lateral drift of vehicles are determined as means to evaluate the lateral stability of vehicles. The utility truck of rear-wheel drive (RWD) is researched, which is high accident rate. Human-vehicle-road simulation models are established by CarSim. Through the orthogonal experiment method, the effects of different road geometries, speed, and interaction factors between road geometries on vehicle lateral stability are studied. In this paper, skidding risk of the vehicle is characterized by the Side-way Force Coefficient (SFC). Rollover risk of the vehicle is characterized by lateral acceleration and the load transfer ratio. Lateral drift risk of the vehicle is characterized by the sideslip angle of wheels. The results of orthogonal analysis reveal that the maximum tire-road friction coefficient and speed are highly significant in skidding of the vehicle. The effects of the combination of horizontal alignment and superelevation on vehicle skidding are important. The effects of horizontal alignment and speed on vehicle rollover risk are highly significant. The effects of superelevation on vehicle rollover risk are significant. The effects of the interaction of horizontal alignment and superelevation are also important on vehicles' rollover risk. The speed and the maximum tire-road friction coefficient have highly significant effect on the vehicle's lateral drift. The superelevation has a significant effect on the vehicle's lateral drift. The effects of the interaction of horizontal alignment and superelevation and longitudinal slope are also important on the lateral drift of the vehicle.

1. Introduction

Road accidents caused by lateral stability of the vehicle have always been a tough concern of vehicle safety in the world. In order to solve this problem, many experts and scholars work on studying how to reduce or even avoid the safety risk caused by lateral stability. The significant results have been achieved, but traffic accidents are still serious. The latest statistical data from the National Highway Traffic Safety Administration of United States [1] are shown in Table 1. Of 52,200 fatal automotive vehicle accidents, 31.5% of death toll was caused by rollover [1]. The number of rollover occurrence caused by single-vehicle crashes is greater than multiple-vehicle crashes. Therefore, there is an urgent need to investigate the accident of rollover caused by single-vehicle crashes.

In the recent years, study on lateral stability of vehicles mainly focus on driving assistance using a vehicle stability control system, such as an antilock brake system (ABS), electronic stability controller (ESC), and acceleration slip regulation (ASR). When vehicles are in the transverse unstable state, the vehicle stability control system actively controls and corrects vehicle movement [2–5]. These systems have brought about a striking effect in antisideslip. However, most of the driving assistance systems are concerned about the antiskid risk of vehicles, paying less attention to the hidden dangers caused by vehicle rollover. Relying on the vehicle stability control system only cannot

Table 1: United States Traffic Accident Statistics [1].

Vehicle type	Rollover occurrence caused by single-vehicle crashes (%)	Rollover occurrence caused by multiple-vehicle crashes (%)	Death toll caused by rollover (%)
Passenger car	41.7	7.1	22
Light truck-pickup	57.1	21.6	43.3
Light truck-utility	64.7	26.6	48.5
Light truck-van	50	16	28
Other	63.8	25	
Total	50.9	12.9	31.5

solve the road traffic safety problems completely. More attention needs to be paid to the ultimate and different causes of road traffic accidents [6].

Road traffic accidents are mainly caused by three factors: roads, drivers, and vehicles. Road environment-related factors cause 27% of accidents in the United States [7]. Road geometric factors cause 34% of vehicle collisions in the United States and Britain [8]. These studies show that bad road conditions or improperly designed roads are the major causes of vehicle accidents [9].

The shortcomings of the existing research on the impact of road factors on vehicle accidents caused by lateral stability are reflected in threefold.

Firstly, the method of the influence of road geometry on vehicle safety is mainly the accident black spot analysis method. That is to say, accident statistics are carried out for accident-prone roads [10]. The references were seldom on the effect of road geometry on vehicle dynamics and, then, extended to vehicle lateral stability.

Secondly, the existing research studies on the effect of road geometry on vehicle lateral stability mainly consider vehicle rollover or skidding. Vehicle lateral drift has not been taken into account. It has not been reported that the three indexes of rollover, skidding, and lateral drift are considered at the same time. Stergios Mavromatis focuses on the study of road factors on vehicle skidding and stopping sight distance [11–13]. Our research group has systematically studied the influence of road geometry, skid resistance, sight distance, and three-dimensional vision on vehicle rollover, skidding, and stopping sight distance [14–16].

Thirdly, the existing road design parameters based on the mass point model of are designed. The radius parameters of curves are based on the minimum radius formula (1) of curves based on the classical mass point model in highway design code. The model ignores the parameter differences between vehicles, such as vehicle type, mass, and center of gravity position.

$$R = \frac{V^2}{127\left(f_R + e\right)}, \tag{1}$$

where f_R—lateral friction demand of the mass point model, V(km/h)—vehicle speed, R(m)—the radius of a circular curve, and e—superelevation.

Based on the NHTSA data [1], 95% of 522,000 automotive vehicle accidents are passenger cars or light trucks. As shown in Table 1, compared with passenger cars, pickup, vans, large trucks, and buses, utility trucks have the highest rollover occurrence caused by single-vehicle crashes (64.7%). Based on the analysis of vehicle accidents and the shortcomings of existing researches, this paper takes the utility trucks as the research target. A human-vehicle-road simulation model is established by CarSim. The orthogonal experimental method is adopted. Through orthogonal experiment, the effects of different road geometries, speed, and interaction factors on vehicle lateral stability are studied. Significance analysis of skidding, rollover, and lateral drift are carried out to characterize vehicle lateral stability.

2. Methods

2.1. Road Model. The road geometric alignment mainly includes horizontal alignment, longitudinal slope, superelevation, road crown, and their combination. The horizontal alignment is shown in Figure 1(a), which usually consists of straight lines, transition curves, and circular curves. The radius of the circular curve is R. The longitudinal slope includes straight lines and vertical curves, as shown in Figures 1(b) and 1(c). It refers to the ratio of the height difference of two points of the same slope to its horizontal distance on the vertical section of a route [17]. Longitudinal slope is expressed by i_{slope}. In order to offset part or even all of the centrifugal force generated while vehicles negotiate a curve, the curve section is usually designed to a one-way cross slope with lateral high and medial low. It is called superelevation. As shown in Figure 1(d), the superelevation slope is $i_{\text{superelevation}}$. In order to facilitate the drainage of the road surface, the road is designed into an arch with high center and low sides, which is called the road crown. As shown in Figure 1(e), the gradient is i_0. The slope is called as the composite longitudinal slope with overlapping superelevation and of longitudinal slope sections, as shown in Figure 1(f). The formula of calculating the composite longitudinal slope is [17]

$$i_{\text{combination}} = \sqrt{i_{\text{superelevation}}^2 + i_{\text{slope}}^2}. \tag{2}$$

Because of the superelevation and longitudinal slope are small in road design code, the angle of the road's cross slope is approximately equal to the superelevation $e \approx i_{\text{superelevation}}$. For the same reason, the angle of the longitudinal slope is approximately equal to its longitudinal slope $e \approx i_{\text{slope}}$. The

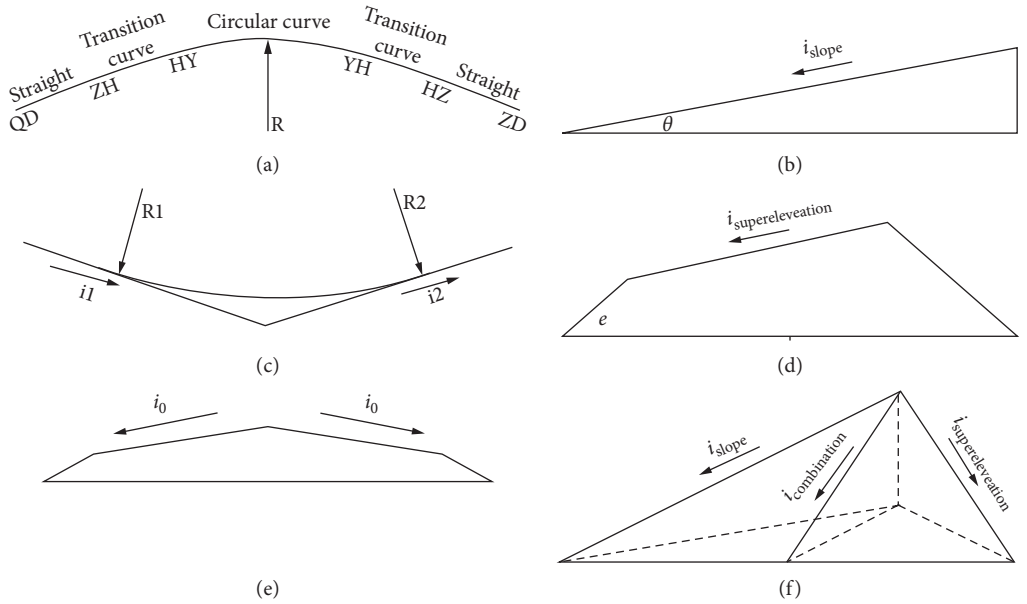

Figure 1: Road geometric design. (a) Horizontal curve. (b) Longitudinal slope. (c) Vertical curve. (d) Superelevation. (e) Road crown. (f) Composite longitudinal slope.

angle of the composite longitudinal slope is approximately equal to its longitudinal slope $\theta_c \approx i_{\text{combination}}$.

2.2. Vehicle Model

2.2.1. Full Vehicle Model. In the past two decades, experts and scholars have developed various vehicle dynamics models [12]: the mass point model, bicycle model [18, 19], 8 degrees of freedom model [20], and 11 degrees of freedom model [21]. The complexity of the models increases gradually. ADAMS is a multibody dynamics simulation tool developed by MSC Software. The main function of ADAMS is to model and simulate multibody dynamics. The vehicle dynamics module of ADAMS/Car can be used for vehicle performance simulation. However, the complexity of the vehicle modeled by ADAMS/Car is very high, and the simulation speed may be very slow. The multibody vehicle simulation software CarSim developed by UMTRI is mainly used in the automobile industry. The software has been validated for many years. The simplified model includes 27 degrees of freedom. The stability and reliability of the model are very high, and the simulation speed is fast.

The vehicle types studied in this paper are light truck-compact utility defined in CarSim [1, 22]. CarSim simplifies the vehicle model into 10 parts: one body part, four unsprung mass parts, four wheel parts, and one engine crankshaft part. The simplified model consists of 27 degrees of freedom, as shown in Figure 2(a): three degrees of freedom of movement (x, y, z), three degrees of freedom of rotation (X, Y, Z), four degrees of freedom of unsprung mass, four degrees of freedom of wheels, one degree of freedom of the transmission system, eight degrees of freedom of transient characteristics of tires, and four degrees of freedom of braking pressure. Specifically, vehicle modeled by CarSim is shown in Figure 2(b). The model includes seven subsystems: the body, aerodynamics, transmission assembly, brake system, steering system, tire, and suspension. In this paper, the utility truck of the rear-wheel drive is selected as the research target. The specific parameters of the utility truck are shown in Table 2 [21, 22].

2.2.2. Tire Model. The "Magic Formula" tire model of Pacejka [23–25] with high fitting accuracy is used in this paper. The expressions are as follows:

$$y = D\sin\{C\arctan[Bx - E(Bx - \arctan Bx)]\}. \tag{3}$$

In the formula, y can be a longitudinal force, a lateral force, or an aligning torque, while the independent variable can represent the sideslip angle or the longitudinal slip rate of the tire in different cases. Based on our previous research [26], this paper considers the tire with good quality as the research object, ignoring the zero drift in the horizontal and vertical directions of tires. The longitudinal force formula under the pure slip condition is fitted by the algebraic polynomial method [27, 28]:

$$F_x(\lambda) = D_x\sin\left(C_x\arctan\left(B_x\lambda - E_x\left(B_x\lambda - \arctan\left(B_x\lambda\right)\right)\right)\right), \tag{4a}$$

where $C_x = P_{Cx1}$, $D_x = (P_{Dx1} + P_{Dx2}df_z)\cdot F_z$, $E_x = P_{Ex1} + P_{Ex2}df_z$, $K_x = F_z\cdot(P_{Kx1} + P_{Kx2}df_z)\cdot\exp(P_{Kx3}df_z)$, and $B_x = (K_x/(C_xD_x))$.

Under the condition of pure sideslip, the formula of lateral force is as follows:

$$F_y(\alpha) = D_y\sin\left(C_y\arctan\left(B_y\alpha - E_y\left(B_y\alpha - \arctan\left(B_y\alpha\right)\right)\right)\right), \tag{4b}$$

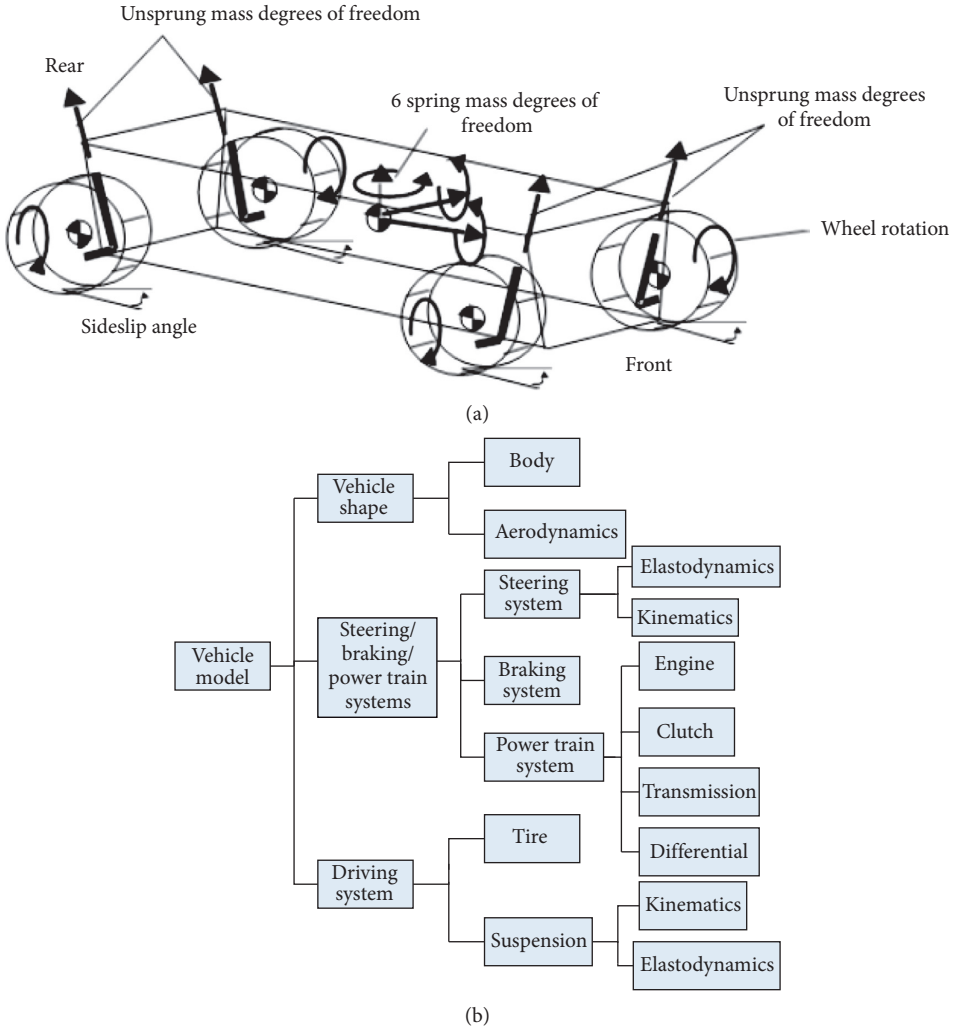

Figure 2: (a) Twenty-seven DOFs vehicle model. (b) CarSim vehicle structure.

Table 2: Vehicle simulation parameters [21, 22].

Parameter (unit)	Value (utility vehicle)
Sprung mass m_s (kg)	600
Full vehicle m (kg)	768
Moment of inertia of sprung mass around X-axis I_{xx} (kg.m^2)	384.0
Moment of inertia of sprung mass around Y-axis I_{yy} (kg.m^2)	624.2
Moment of inertia of sprung mass around Z-axis I_{zz} (kg.m^2)	686.9
Horizontal distance between the center of mass and front wheels a (mm)	550
Horizontal distance between the center of mass and rear wheels b (mm)	1373
Centroid height h (mm)	700
The height between the center of mass and the center of roll h_c (mm)	573
Front wheelbase c_f (mm)	1260
Rear-wheelbase c_r (mm)	1260
Wheel radius R (mm)	347
Wheel moment of inertia I_w (kg.m^2)	0.9

where $C_y = P_{Cy1}$, $D_y = (P_{Dy1} + P_{Dy2}df_z) \cdot F_z$, $E_y = P_{Ey1} + P_{Ey2}df_z$, $K_y = P_{Ky1} \cdot F_{z0} \cdot \sin\{2\tan^{-1}[(F_z/(P_{Ky2}F_{z0}))]\}$, and $B_y = (K_y/(C_yD_y))$.

Here, α is the wheel sideslip angle, λ is the wheel slip rate, $F_x(\lambda)$ is the longitudinal force calculated in the pure slip condition, $F_y(\alpha)$ is the lateral force of the tire in pure

sideslip movement, and F_z is the vertical force of the tire; the value of fitting parameters is shown in Table 3.

2.3. Driver Model. There are two kinds of vehicle dynamics simulation systems: the open-loop simulation system and closed-loop simulation system. The open-loop simulation system regards the vehicle itself as an independent control system. The system does not consider the driver's feedback characteristics, as shown in Figure 3(a). The closed-loop simulation system incorporates the driver's feedback into the system. The driver continuously corrects the steering wheel angle through track estimation to form a closed-loop system, as shown in Figure 3(b). The closed-loop system can simulate the influence of road factors on vehicle dynamics more realistically. In this paper, a closed-loop simulation optimal preview model raised by Charles C. Macadam is used, which can correct the trajectory [22, 29, 30]. Drivers get information about the road ahead and vehicles through "preview" and "perception". Drivers make judgments based on the acquired information and adjust the motion state of vehicles. This forms a closed system.

The station formula of the target position [22] is

$$S_{t\text{arg},i} = S + \frac{iV_x T}{m}. \tag{5}$$

S refers to the station of the center line of the road's horizontal geometric figure defined by coordinates X and Y. For any station S, it corresponds to unique X and Y coordinates. Route S is defined as a function of X and Y through a linear connection point. For each pair of X–Y coordinates, the Pythagorean theorem is used to calculate the corresponding s-increment.

$$S_i = S_{i-1} + \sqrt{(X_i - X_{i-1})^2 + (Y_i - Y_{i-1})^2}. \tag{6}$$

The calculation of the controller uses a special coordinate axis system, as shown in Figure 4. In this coordinate axis, the center of the front axle of the vehicle should be located at $x = 0$ and $y = 0$. The yaw angle of a vehicle is defined as $\psi = 0$, the alignment of the X and Y axles with the longitudinal and lateral axes of the vehicle, respectively. In the coordinate axes of the driver's controller, the motion of the vehicle is predicted based on these axes. The axis is fixed in the inertial reference and rotates ψ degree based on the inertial axis.

The target translates transversely in this coordinate system. First, the inertia of X and Y coordinates of the path are calculated as the path function of the target position (Starg). Then, applying the transformation [22],

$$Y_{t\text{arg}} = \left[Y\left(S_{t\text{arg}}\right) - Y_V\right]\cos(\psi) - \left[X\left(S_{t\text{arg}}\right) - X_V\right]\sin(\psi). \tag{7}$$

Within the coordinate range of the steering controller, the vehicle is always at the origin of the axis shown in Figure 4. The time is 0, and the target path is known from time 0 to preview time T.

Table 3: Fitting parameters of the "Magic Formula" [20].

P_{Cx1}	P_{Dx1}	P_{Dx2}	P_{Ex1}	P_{Ex2}	P_{Kx1}	P_{Kx2}	P_{Kx3}
1.62	1.035	−0.0487	0.5	−0.122	19.4	−0.13	0.171
P_{Cy1}	P_{Dy1}	P_{Dy2}	P_{Ey1}	P_{Ey2}	P_{Ky1}	P_{Ky2}	
1.29	−0.9	0.18	−1.07	0.68	−12.95	1.72	

3. Safety Margin Analysis of Lateral Stability

This paper uses the safety margin from our previous study as a variable to reflect the extent of the index approaching the threshold. As shown in Figure 5, the safety margin-station curve of the vehicle dynamics index is obtained from the vehicle dynamics simulation. It can be seen that the larger the value of $I_j(t)$ is, the closer it is to the threshold I_j^0 and the greater the possibility of rollover, skidding, and lateral drift are. Therefore, this paper uses formula (8) to define the safety margin of index J to measure the probability of accident risk caused by lateral unstability of vehicles.

$$M_j = I_j^0 - \max\left(\left|I_j(t)\right|\right), \quad 0 \le M_j \le I_j^0. \tag{8}$$

3.1. Safety Margin of Vehicle Skidding Risk. When a vehicle is traveling on a curve, the lateral force perpendicular to the direction of the vehicle will be produced due to the influence of centrifugal force and cross slope. When the lateral force is equal to or exceeds the maximum lateral adhesion force provided by the road surface, it will cause lateral slip of one or both axles of the vehicle, which is called skidding. Vehicle skidding includes skidding of four wheels, skidding of the front wheel, and skidding of the rear wheels. The phenomenon that the trajectory tracking ability is lost due to the skidding of the front axle in a curve is called the front-wheel skidding.

The phenomenon of instability caused by skidding of four wheels is called lateral drift [31]. Lateral drift is studied separately below. According to the definition of the skidding, the lateral force coefficient of wheels is taken as the indicator of vehicle skidding in this paper. The lateral force coefficient [32] formula of the vehicle is

$$\mu_l = \max\left(\left|\frac{F_{yi}}{F_{Zi}}\right|\right), \quad i = 1, 2, 3, 4, \tag{9}$$

where F_{yi} is the tire lateral force, F_{Zi} is the tire vertical force, $i = 1$, 2, 3, 4 are the left-front wheel, left-rear wheel, right-front wheel, and right-rear wheel, respectively;

When the lateral force coefficient of any wheel is greater than the lateral maximum tire-road friction coefficient, the vehicle will skid. Let μ_l^0 be the adhesion coefficient provided by the pavement when skidding is about to occur. It also requires the lateral maximum tire-road friction coefficient to avoid skidding. When $\mu_l > \mu_l^0$, skidding will occur. The tested maximum tire-road friction coefficient f_p is 0.8, 0.5, and 0.2 [32], which correspond, respectively, to dry, wet, and snow conditions of the asphalt pavement. According to [33], the lateral maximum tire-road friction $f_{R\max} = 0.925 f_p$.

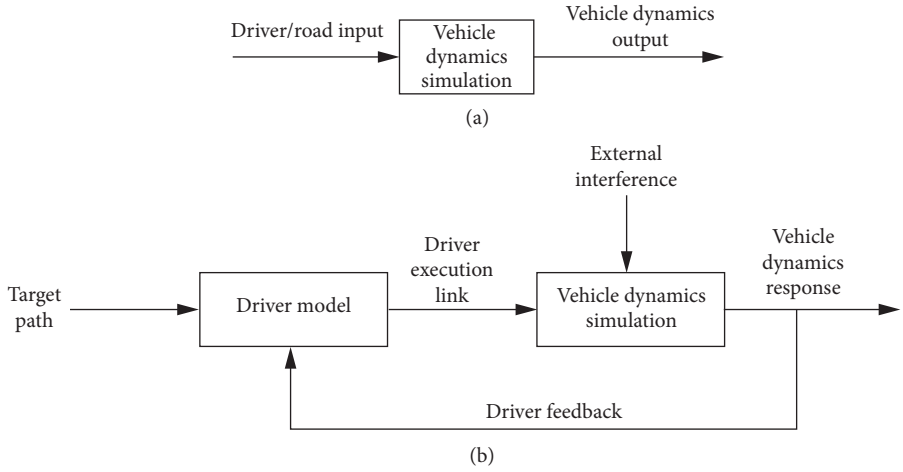

Figure 3: Flow chart of simulation. (a) Open-loop simulation. (b) Closed-loop simulation.

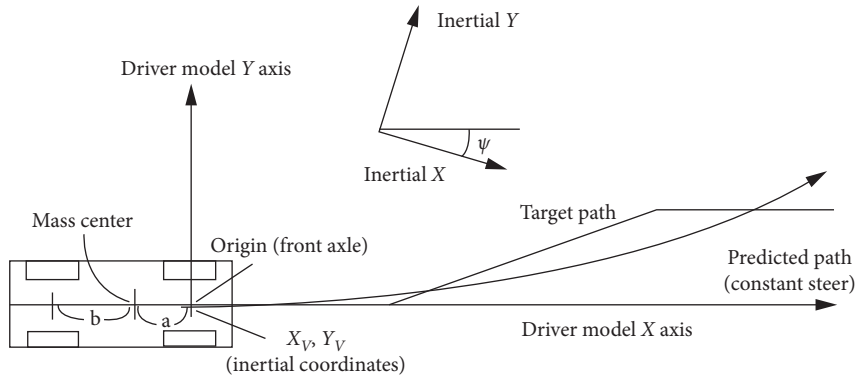

Figure 4: Axis system of the steering controller.

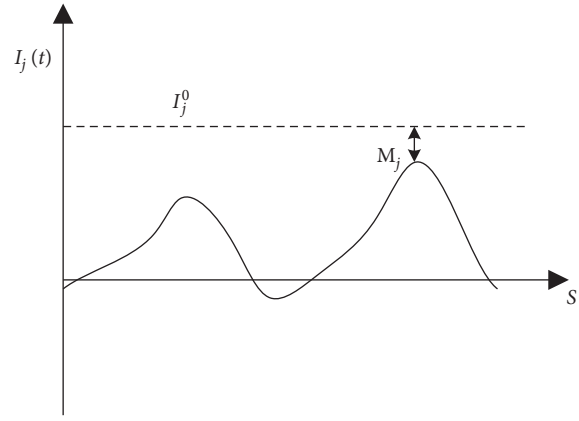

Figure 5: The station curve of index j.

However, the vehicle is at a high slip value in this paper, and the brake is blocked or the slip is accelerated [32, 34]. In such a situation, the maximum tire-road friction coefficient is equivalent to the sliding adhesion coefficient f_s. Namely, $f_p = f_s$. Therefore, $f_{R\max} = 0.925 f_s$. Table 4 shows the maximum tire-road friction coefficients, slip friction coefficient, and lateral maximum tire-road friction coefficient of asphalt pavements under dry, wet, and snow conditions.

The safety margin of vehicle skidding on curves is defined as the difference between the lateral maximum tire-road friction coefficient provided by the available tire-road and the lateral friction demand [35]. So, the corresponding safety margin of vehicle skidding is obtained:

$$M_1 = \mu_l^0 - \max(\mu_l), \quad 0 \le M_1 \le \mu_l^0. \tag{10}$$

Table 4: The maximum tire-road friction coefficients, slip friction coefficient, and lateral maximum tire-road friction coefficient [32–34].

Maximum tire-road friction coefficients	Slip friction coefficient	Lateral maximum tire-road friction coefficient
f_p	f_s	$f_{R\max} = 0.925 f_s$
0.8	0.75	0.69
0.5	0.45	0.41
0.2	0.15	0.13

f_p: maximum tire-road friction coefficient; f_s: slip friction coefficient; the slip friction coefficient is equal to the braking force coefficient when the sliding rate is 100%. $f_{R\max}$: lateral maximum tire-road friction coefficient.

3.2. Safety Margin of Vehicle Rollover Risk. There are two types of vehicle rollover: nontripping rollover and tripping rollover. When vehicles' lateral acceleration exceeds the compensation limit of lateral tire weight transfer, the vehicle rotates 90 degrees or more around its longitudinal axis, which is called nontripping rollover. Another is that when a vehicle slips, the vehicle loses control. The vehicle is impacted by the cross slope, the curb, and mollisol, so as to "trip" the vehicle, and rotates 90 degrees or more around its longitudinal axis, which is called tripping rollover. Because the risk of skidding occurs before tripping rollover and skidding has been expressed above, this paper only studies nontripping rollover. Based on the abovementioned definition of rollover, the lateral acceleration and load transfer ratio are selected as the indicators to measure vehicle rollover risk. The load transfer ratio is defined as the ratio of the amount of load transferred from the inside to the outside to the total load [36], as shown in the following equation:

$$\mathrm{LTR} = \frac{\sum_{i=1}^{2}\left[\left(F_{ZR}\right)_i - \left(F_{ZL}\right)_i\right]}{\sum_{i=1}^{2}\left[\left(F_{ZR}\right)_i + \left(F_{ZL}\right)_i\right]}. \tag{11}$$

When the inner wheel load is zero, that is, the inner vehicle leaves the ground, at this time, LTR = 0, and the threshold of the load transfer ratio is, thus, obtained. The corresponding safety margin of rollover is

$$M_2 = \mathrm{LTR}^0 - \max\left(\left|\mathrm{LTR}\left(t\right)\right|\right), \quad 0 \le M_2 \le \mathrm{LTR}^0. \tag{12}$$

In this paper, the quasistatic model of a rigid vehicle is used. The rigid vehicle means neglecting the elastic deformation of the vehicle and tire [32]. Quasistatic refers to the vehicle steady-state steering [32]. The quasistatic model of a rigid vehicle is shown in Figure 6. The torque formula of the contact point between the outside wheel and the ground is as follows:

$$\left(F\cos\alpha - mg\sin\alpha\right)h_g + N_{xi}\cdot B - \left(F\sin\alpha + mg\cos\alpha\right)\cdot\frac{B}{2} = 0. \tag{13}$$

Here, F is the centrifugal force; α is the bank angle of roads; N_{yi} and N_{y0} are the lateral forces on the inner and outer tires, respectively; N_{xi} and N_{x0} are the vertical forces on the inner and outer tires, respectively; a_y is the lateral acceleration; and B is the wheel base.

As the bank angle α of the road is generally small, $\sin\alpha \approx \tan\alpha = \alpha = i_{\text{superelevation}}$, $\cos\alpha \approx 1$. Moreover,

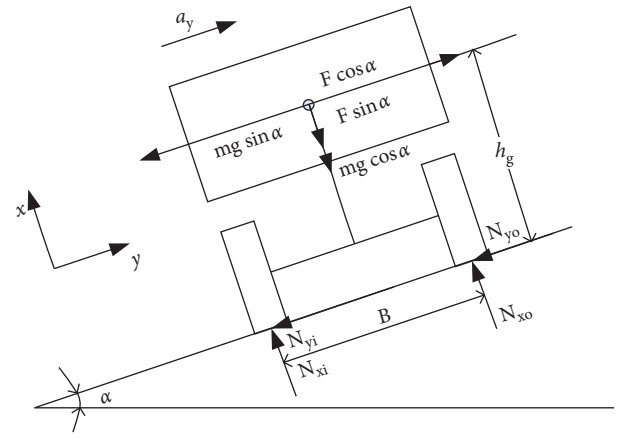

Figure 6: The free-body diagram of the quasistatic model of a rigid vehicle.

$F\cos\alpha - mg\sin\alpha = ma_y$, which can be derived from equation (13) as follows:

$$ma_y h_g + N_{xi}\cdot B - \left(F\alpha + mg\right)\cdot\frac{B}{2} = 0. \tag{14}$$

When N_{xi} becomes 0, the vehicle begins to rollover. The lateral acceleration when the vehicle begins to rollover is called the rollover threshold, which can be derived from equation (14) as follows:

$$a_y = \frac{F\alpha + mg\cdot\left(B/2\right)}{mh_g}. \tag{15}$$

Clearly, when the bank angle is $\alpha = 0$, the rollover threshold is $a_y = (B/2h_g)g$. The parameters in Table 2 are substituted into equation (15) to obtain the resulting rollover threshold $a_y = 0.9g$. The quasistatic model of the rigid vehicle is reasonable only when the lateral acceleration changes slowly [32]. When the lateral acceleration changes rapidly, a physical model of roll is needed. However, modeling is not critical in this paper, and this paper directly applies the conclusion of [32]. For the utility truck, the rollover threshold value of the physical model of roll is lower 30% than that of the quasistatic model of rigid vehicle [32]. Therefore, the rollover threshold value of the physical model of roll is $a_y^0 = (1 - 30\%)\cdot a_y = 0.63g$, which can be derived from equation (8) as follows:

$$M_3 = a_y^0 - \max\left(\left|a_y\left(t\right)\right|\right), \quad 0 \le M_3 \le a_y^0. \tag{16}$$

3.3. Safety Margin of the Vehicle's Lateral Drift Risk. High sideslip cornering is also called drift [37]. When vehicles are traveling in curves when the speed is too high (e.g., racing activities) or the radius of the curves is too small, their wheels will lose grip. The sideslip angle of the vehicle exceeds its control limit, and the vehicle runs at the tire-road adhesion limit [38]. At this time, the vehicle is turning in the opposite direction of bend with large sideslip angle, and the

wheels are nearly saturated. This state of the vehicle is called drift [39].

According to the definition of lateral drift, the sideslip angle of a vehicle is determined as the indicator of vehicle lateral drift. Sideslip angle is the angle between the direction of movement of the wheel center and the lateral velocity [34, 37]. The expression is as follows:

$$\beta = \arctan\frac{V_y}{V_x}, \tag{17}$$

where β- vehicle sideslip angle; V_y- lateral speed of the tire-road contact point; and V_x- longitudinal speed of the wheel rotation center.

Based on the literature of Yu [32] and the definition of lateral drift, when the lateral friction coefficient of the rear wheels of the vehicle reaches the critical value of skidding, the rear wheel is close to saturation state, and the sideslip angle at this time is defined as the threshold of lateral drift. The road model is developed by CarSim. The radius of the road is designed as 250 m, the longitudinal slope is designed as 0.06, and the superelevation is designed as 0.08 (the road model is the most unfavourable road condition on the basis of <Highway Engineering Technology Standard (JTG B 01-2014) > when the design speed is 80 km/h.). The peak adhesion coefficient of the pavement is 0.8, 0.5, and 0.2. The vehicle speed starts at 80 km/h, and increases continuously every other 5 km/h until the vehicle is about to skid. At this time, the vehicle's sideslip angle is 3.71°, 2.34°, and 0.59 , respectively, and this value is defined as the lateral drift threshold of vehicles. The safety margin of lateral drift of the vehicle is

$$M_4 = \beta^0 - \max(|\beta|), \quad 0 \le M_4 \le \beta^0. \tag{18}$$

4. Numerical Analysis

4.1. Orthogonal Experimental Design with Interaction. In this paper, the method orthogonal experimental design is used to analyze the influence of the road's horizontal alignment (A), longitudinal slope (B), superelevation (C), maximum tire-road friction coefficient (D), and vehicle speed (E) on vehicle lateral stability. The interaction of horizontal alignment and the longitudinal slope (AB), the interaction of horizontal alignment and superelevation (AC), and the interaction of horizontal alignment and the pavement friction coefficient (AD) are also considered. The levels of factors are shown in Table 5, and each factor contains three levels. The orthogonal table of $L_{27}(3^{13})$ (this form can be seen in the supplementary document (Experimental data). The supplementary document is the selected orthogonal table and the experimental data for orthogonal analysis) is selected in this paper. Based on literature [40], we can get the location of the interaction factors column. The header's design of the table is shown in Table 6, with blank columns as error items.

4.2. Analysis of Experimental Results. Tables 7–10 are the variance analysis table of skidding's safety margin, rollover's safety margin, and lateral drift's safety margin. The influence of some factors on the experimental results is not obvious. Namely, mean square value $\overline{S_j} < \overline{S_e}$. Therefore, the sum of squares of row of these factors' location is incorporated into the error line e, and a new error line is obtained. As shown in Table 7, $\overline{S_A} < \overline{S_e}$, $\overline{S_B} < \overline{S_e}$, $\overline{S_{A\times B}} < \overline{S_e}$, $\overline{S_{A\times D}} < \overline{S_e}$; therefore, we should incorporate S_A, S_B, $S_{A\times B}$, $S_{A\times D}$ into S_e. New sum of squares of errors and degrees of freedom are obtained. $S_{e^\Delta} = S_e + S_A + S_B + S_{A\times B} + S_{A\times D}$ and $f_{e^\Delta} = f_e + f_A + f_B + f_{A\times B} + f_{A\times} D$. Analysis of variance is carried on by the formula $F = ((S_j/f_j)/(S_{e^\Delta}/f_{e^\Delta}))$. If $F \ge F_{1-\alpha}(f_j, f_{e^\Delta})$, the significance of this factor on the experimental results is inferred from the significance α. If $F_j \ge F_{1-0.01}(f_j, f_{e^\Delta})$, the influence of this factor on the experimental results is highly significant. If $F_{1-0.01}(f_j, f_{e^\Delta}) > F_j \ge F_{1-0.05}(f_j, f_{e^\Delta})$, the influence of this factor on the experimental results is significant. If $F_{1-0.05}(f_j, f_{e^\Delta}) > F_j \ge F_{1-0.1}(f_j, f_{e^\Delta})$, the influence of this factor on the experimental results is commonly significant. If $F_{1-0.1}(f_j, f_{e^\Delta}) > F_j$, the influence of this factor on the experimental results is not significant. For the same reason, Tables 8–10 are available.

For the safety margin of skidding M1, analysis of variance based on orthogonal Table 6 is carried on. Because the skidding safety margin obtained is small, the original value is multiplied by 1000 in the calculation process. Table 7 is $F_D > F_{1-0.01}(2, 16)$ obtained by the analysis of variance. In the table, $F_{1-0.01}(2, 16) > F_C \ge F_{1-0.05}(2, 16)$, $F_D > F_{1-0.01}(2, 16)$, $F_E > F_{1-0.01}(2, 16)$, and $F_{AC} < F_{1-0.1}(2, 16)$, it shows that the maximum tire-road friction coefficient and vehicle speed have a highly significant influence on the vehicle's lateral force coefficient. That is to say, the impact on vehicle skidding is highly significant. The superelevation has a significant influence on the vehicle's lateral force coefficient. That is to say, the impact on vehicle skidding is significant. Other factors have no significant effect on vehicle skidding.

In this paper, the range R_j of the safety margin of skidding is calculated to determine the order of primary and secondary factors affecting skidding. From main to secondary, $R_D > R_E > R_{AC} > R_C > R_{AB} > R_A > R_B > R_{AD}$. Obviously, except for a single factor, the maximum tire-road friction coefficient, vehicle speed, and superelevation, the interaction of horizontal alignment and superelevation has an important effect on vehicle skidding. It cannot be ignored.

The results from two analyses suggest that the maximum tire-road friction coefficient and vehicle speed have a highly significant effect on vehicle skidding. The superelevation has a significant influence on the vehicle's skidding. The interaction of horizontal alignment and superelevation has an important influence on vehicle's skidding.

Figure 7 shows the effect of the significant single factor on the safety margin of vehicle skidding. Figure 7(a) shows the effect of superelevation on the safety margin of vehicle skidding. The speed $v = 100$ (km/h), radius of the circular curve $R = 700$ m, and the maximum tire-road friction coefficient $f_p = 0.8$. The 600 m−1200 m road section is selected as the research object. The 600–800 m road section is the transition section from a straight line to a circular curve (clothoid curve section). The 800–1200 m road section is a circular curve section. The values of superelevation are

Table 5: Factors and level table [40].

Level	A Horizontal alignment (m)	B Grade (%)	C Superelevation (%)	D Maximum tire-road friction coefficient	E Speed (km/h)
1	700	−4	4	0.2	80
2	1000	0	6	0.5	100
3	1500	4	8	0.8	120

Table 6: Header's design with factors interaction and mixed levels.

Factor	A	B	$(AB)_1$	$(AB)_2$	C	$(AC)_1$	$(AC)_2$	D	$(AD)_1$	$(AD)_2$	E		
Column	1	2	3	4	5	6	7	8	9	10	11	12	13

Table 7: The table of variance analysis of skidding's safety margin M_1.

Sources of variation	Square sum S_j	Freedom f	Mean square $\overline{S_j}$	F value	Significance	Critical value
$A^{\triangle}$	3.630	2	1.815			
$B^{\triangle}$	4.519	2	2.259			
C	22.296	2	11.148	4.704	Significant	
D	14507.630	2	7253.815	3060.68	Highly significant	$F_{1-0.05}(2,16) = 3.63$
E	132.741	2	66.370	28.004	Highly significant	$F_{1-0.01}(2,16) = 6.23$
$(A \times B)^{\triangle}$	7.703	4	1.926			$F_{1-0.1}(4,16) = 2.33$
$A \times C$	19.926	4	4.982	2.102	Nonsignificant	$F_{1-0.05}(4,16) = 3.07$
$(A \times D)^{\triangle}$	3.926	4	0.982			
e	18.148	4	4.537			
$e^{\triangle}$	37.926	16	2.370			

Table 8: The table of variance analysis of rollover's safety margin M_2.

Sources of variation	Square sum S_j	Freedom f	Mean square $\overline{S_j}$	F value	Significance	Critical value
$A^{\triangle}$	7.356	2	3.678			
$B^{\triangle}$	6.586	2	3.293			
C	55.352	2	27.676	3.455	Significance	
$D^{\triangle}$	15.278	2	7.639			$F_{1-0.1}(2,22) = 2.56$
E	76.289	2	38.144	4.761	Significance	$F_{1-0.05}(2,22) = 3.44$
$(A \times B)^{\triangle}$	21.514	4	5.379			$F_{1-0.01}(2,22) = 5.72$
$(A \times C)^{\triangle}$	49.634	4	12.406			$F_{1-0.1}(4,22) = 2.22$
$(A \times D)^{\triangle}$	11.623	4	2.906			$F_{1-0.05}(4,22) = 2.82 F_{1-0.01}(4,22) = 4.31$
E	64.258	4	16.065			
$E^{\triangle}$	176.249	22	8.011			

Table 9: The table of variance analysis of rollover's safety margin M_3.

Sources of variation	Square sum S_j	Freedom f	Mean square $\overline{S_j}$	F value	Significance	Critical value
A	16360.93	2	8180.037	99.669	Highly significant	
$B^{\triangle}$	0.069	2	0.345			
C	0.023	2	0.0115			
$D^{\triangle}$	0.041	2	0.0205			$F_{1-0.1}(2,22) = 2.56$
E	19248.217	2	9624.108	117.264	Highly significant	$F_{1-0.05}(2,22) = 3.44$
$(A \times B)^{\triangle}$	0.71	4	0.1775			$F_{1-0.01}(2,22) = 5.72$
$(A \times C)^{\triangle}$	0.117	4	0.029			$F_{1-0.1}(4,22) = 2.22$
$(A \times D)^{\triangle}$	0.092	4	0.023			$F_{1-0.05}(4,22) = 2.82 F_{1-0.01}(4,22) = 4.31$
E	1804.547	4	451.137			
$e^{\triangle}$	1805.599	22	82.072			

$e = 0.04, 0.06, 0.08$. As can be seen in the Figure 7(a), with the increase in superelevation values, the safety margin of vehicle skidding increases. Therefore, it is more difficult for the vehicle to skid.

Figure 7(b) shows the effect of the maximum tire-road friction coefficient on the safety margin of vehicle skidding. The speed $v = 80$ (km/h), radius of the circular curve $R = 700$ m, and the superelevation $e = 0.06$. The

Table 10: The table of variance analysis of the safety margin of vehicle lateral drift M_4.

Sources of variation	Square sum S_j	Freedom f	Mean square $\overline{S_j}$	F value	Significance	Critical value
$A^{\triangle}$	213.504	2	106.752			
$B^{\triangle}$	40.831	2	20.416			
C	442.258	2	221.129	4.48	Significant	$F_{1-0.1}(2,22) = 2.56$
D	447987	2	223993.5	4540.07	Highly significant	$F_{1-0.05}(2,22) = 3.44$
E	2207.725	2	1103.862	22.374	Highly significant	$F_{1-0.01}(2,22) = 5.72$
$(A \times B)^{\triangle}$	38.041	4	9.510			$F_{1-0.1}(4,22) = 2.22$
$(A \times C)^{\triangle}$	275.292	4	68.823			$F_{1-0.05}(4,22) = 2.82 F_{1-0.01}(4,22) = 4.31$
$(A \times D)^{\triangle}$	43.575	4	10.894			
e	474.172	4	118.543			
$e^{\triangle}$	1085.415	22	49.337			

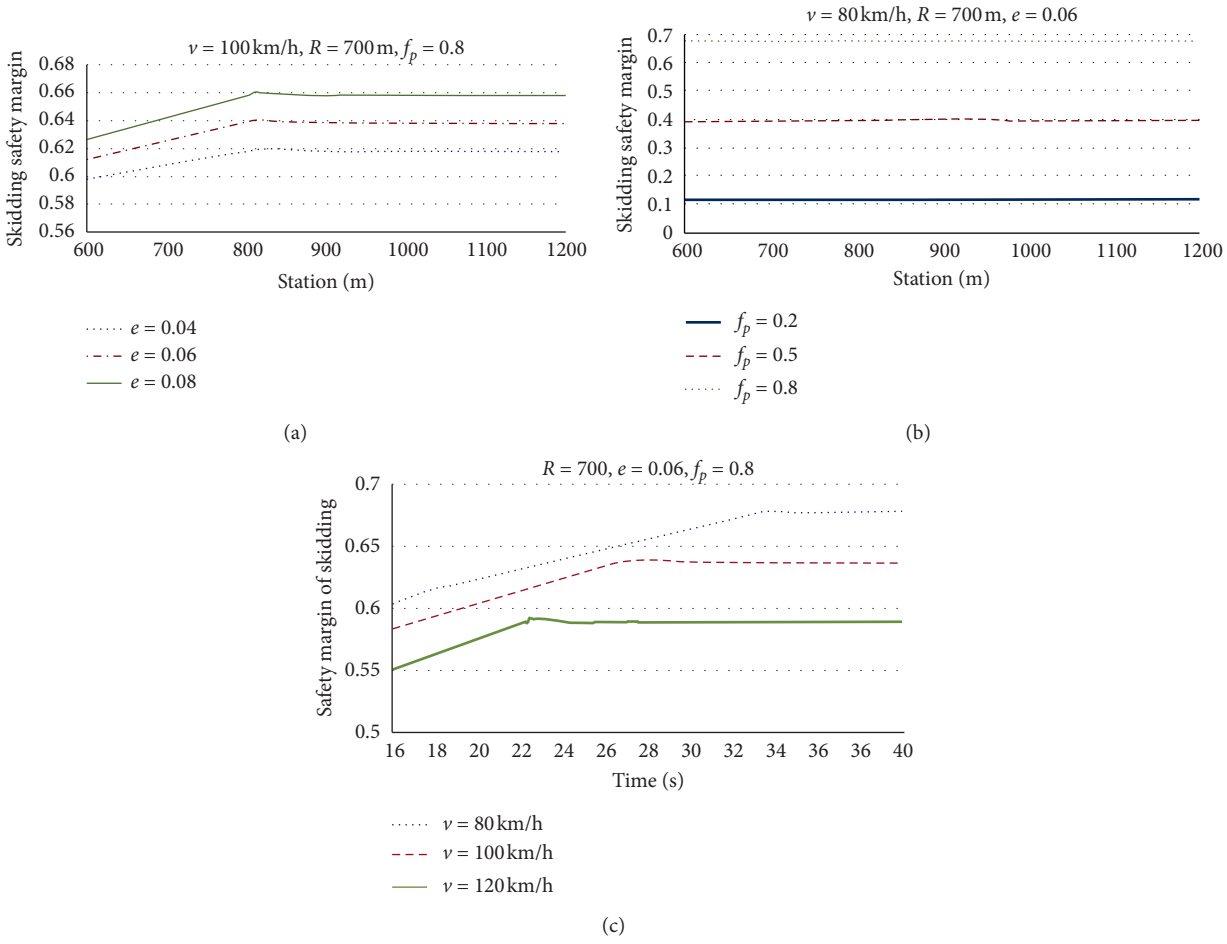

Figure 7: The effect of the significant single factor on the safety margin of the vehicle's skidding. (a) Effect of superelevation on the safety margin of skidding. (b) Effect of the pavement friction coefficient on the safety margin of skidding. (c) Effect of speed on the safety margin of skidding.

600 m–1200 m road section is selected as the research object. The 600–800 m road section is the transition section from a straight line to a circular curve (clothoid curve section). The 800–1200 m road section is a circular curve section. The maximum tire-road friction coefficients are $f_p = 0.2, 0.5, 0.8$. As can be seen from the Figure 7(b), with the increase in the maximum tire-road friction coefficient, the safety margin of vehicle skidding increases. Therefore, it is more difficult for the vehicle to skid.

Figure 7(c) shows the effect of vehicle speed on the safety margin of vehicle skidding. Radius of the circular curve $R = 700$ m, the superelevation $e = 0.06$, and the maximum tire-road friction coefficient $f_p = 0.8$. The road section of time at 16 s–40 s is selected as the research object, which includes two sections: the transition section (clothoid curve section) and circular curve section. The vehicle speeds are $v = 80$ (km/h), 100 (km/h), 120 (km/h). As can be seen from Figure 7(c), with the increase in vehicle speed, the safety

margin of vehicle skidding reduces. Therefore, vehicles are more prone to skidding.

For the safety margin of vehicle rollover M_2, analysis of variance based on orthogonal Table 6 is carried out. Because the safety margin of vehicle rollover obtained is small, the original value is multiplied by 100 in the calculation process. Table 8 is obtained by variance analysis. In the table, $F_C > F_{1-0.05}(2, 22)$, $F_E > F_{1-0.05}(2, 22)$, and it shows that superelevation and vehicle speed have a significant effect on the lateral load transfer ratio of vehicles, that is, the superelevation and vehicle speed have a significant effect on the vehicle's rollover.

In this paper, the range R_j of the safety margin of vehicle rollover is calculated to determine the order of primary and secondary factors affecting rollover. From main to secondary, $R_{AC} > R_E > R_C > R_{AB} > R_{AD} > R_D > R_A > R_B$. Obviously, except for a single factor, superelevation and vehicle speed, the interaction of horizontal alignment and superelevation has a significant effect on vehicle rollover. It cannot be ignored.

For the safety margin of vehicle rollover M_3, analysis of variance based on orthogonal Table 6 is carried out. Because the safety margin of vehicle rollover obtained is small, the original value is multiplied by 1000 in the calculation process. Table 9 is obtained by variance analysis. In the table, $F_A > F_{1-0.01}(2, 22)$, $F_E > F_{1-0.01}(2, 22)$, and it shows that horizontal alignment and vehicle speed have a highly significant effect on the vehicle lateral acceleration. That is, the horizontal alignment and vehicle speed have a highly significant effect on the vehicle's rollover.

The variance analysis from M_2 and M_3 suggests that the horizontal alignment and vehicle speed have a highly significant effect on the vehicle's rollover. The superelevation has a significant influence on the vehicle's rollover. The influence of the interaction of horizontal alignment and superelevation cannot be neglected and also an important factor.

Figure 8 shows the effect of the significant single factor on the safety margin of vehicle rollover. Figure 8(a) shows the effect of superelevation on the safety margin of vehicle rollover (M_2). The speed $v = 100$ (km/h), radius of the circular curve $R = 700$ m, and the maximum tire-road friction coefficient $f_p = 0.8$. The 600 m–1200 m road section is selected as the research object. The 600–800 m road section is the transition section from a straight line to a circular curve (clothoid curve section). The 800–1200 m road section is a circular curve section. The values of superelevation are $e = 0.04, 0.06, 0.08$. As can be seen from Figure 8(a), with the increase of superelevation values, the safety margin of the vehicle's rollover increases. Therefore, vehicles are less prone to rollover.

Figure 8(b) (M_2) and Figure 8(d) (M_3) show the effect of vehicle speed on the safety margin of vehicle rollover. The radius of the circular curve $R = 700$ m, the superelevation $e = 0.06$, and the maximum tire-road friction coefficient $f_p = 0.8$. The road section of time at 16 s–40 s is selected as the research object, which includes two sections: the transition section (clothoid curve section) and circular curve section. The vehicle speeds are $v = 80$ (km/h), 100 (km/h), 120 (km/h). As can be seen from the Figures 8(b) and 8(d), with the increase of vehicle speed, the safety margin of vehicle rollover reduces. Therefore, vehicles are more prone to rollover. As can be seen from Figure 8, the safety margin of vehicle rollover expressed by the load transfer ratio (M_2) is greatly affected by the clothoid curve section, and the rollover safety margin expressed by the lateral acceleration (M_3) is less affected by the clothoid curve section.

Figure 8(c) shows the effect of horizontal alignment on the safety margin of vehicle rollover. The speed $v = 80$ km/h, the superelevation $e = 0.06$, and the maximum tire-road friction coefficient $f_p = 0.8$. The radii of the circular curve are $R = 700$ m, 1000 m, 1500 m. The 600 m–1200 m road section is selected as the research object. The 600–800 m road section is the transition section from a straight line to a circular curve (clothoid curve section). The 800–1200 m road section is a circular curve section. The values of superelevation are $e = 0.04, 0.06, 0.08$. As can be seen from Figure 8(c), with the increase in the radius of the circular curve values, the safety margin of vehicle rollover increases. Therefore, vehicles are less prone to rollover.

For the safety margin of the vehicle's lateral drift M_4, analysis of variance based on orthogonal Table 6 is carried out. Because the safety margin of the vehicle's lateral drift obtained is small, the original value is multiplied by 100 in the calculation process. Table 10 is obtained by variance analysis. In the table, $F_C > F_{1-0.05}(2, 22)$, $F_D > F_{1-0.01}(2, 22)$, $F_E > F_{1-0.01}(2, 22)$, and it shows that the superelevation has a significant effect on the vehicle sideslip angle. Therefore, the superelevation has a significant effect on the vehicle's lateral drift. The vehicle speed and maximum tire-road friction coefficient have a highly significant effect on the vehicle sideslip angle. Therefore, the vehicle speed has a highly significant effect on the vehicle's lateral drift.

In this paper, the range R_j of the safety margin of the vehicle's lateral drift is calculated to determine the order of primary and secondary factors affecting the vehicle's lateral drift. From main to secondary, $R_D > R_B > R_E > R_{AC} > R_C > R_{AD} > R_A > R_{AB}$. Obviously, except for a single factor, superelevation, vehicle speed, and maximum tire-road friction coefficient, the interaction of horizontal alignment and superelevation also have an important effect on the vehicle's lateral drift. It cannot be ignored.

The results from two analyses suggest that the vehicle speed and maximum tire-road friction coefficient have a highly significant effect on the vehicle's lateral drift. The superelevation has a significant effect on the vehicle's lateral drift. The interaction of horizontal alignment and superelevation and longitudinal slope has an important effect on the vehicle's lateral drift. It cannot be ignored.

Figure 9 shows the effect of the significant single factor on the safety margin of the vehicle's lateral drift. Figure 9(a) shows the effect of superelevation on the safety margin of the vehicle's lateral drift. The speed $v = 100$ (km/h), radius of the circular curve $R = 700$ m, and the maximum tire-road friction coefficient $f_p = 0.8$. The 600 m–1200 m road section is selected as the research object. The 600–800 m road section is the transition section from a straight line to a circular curve (clothoid curve section). The 800–1200 m road section

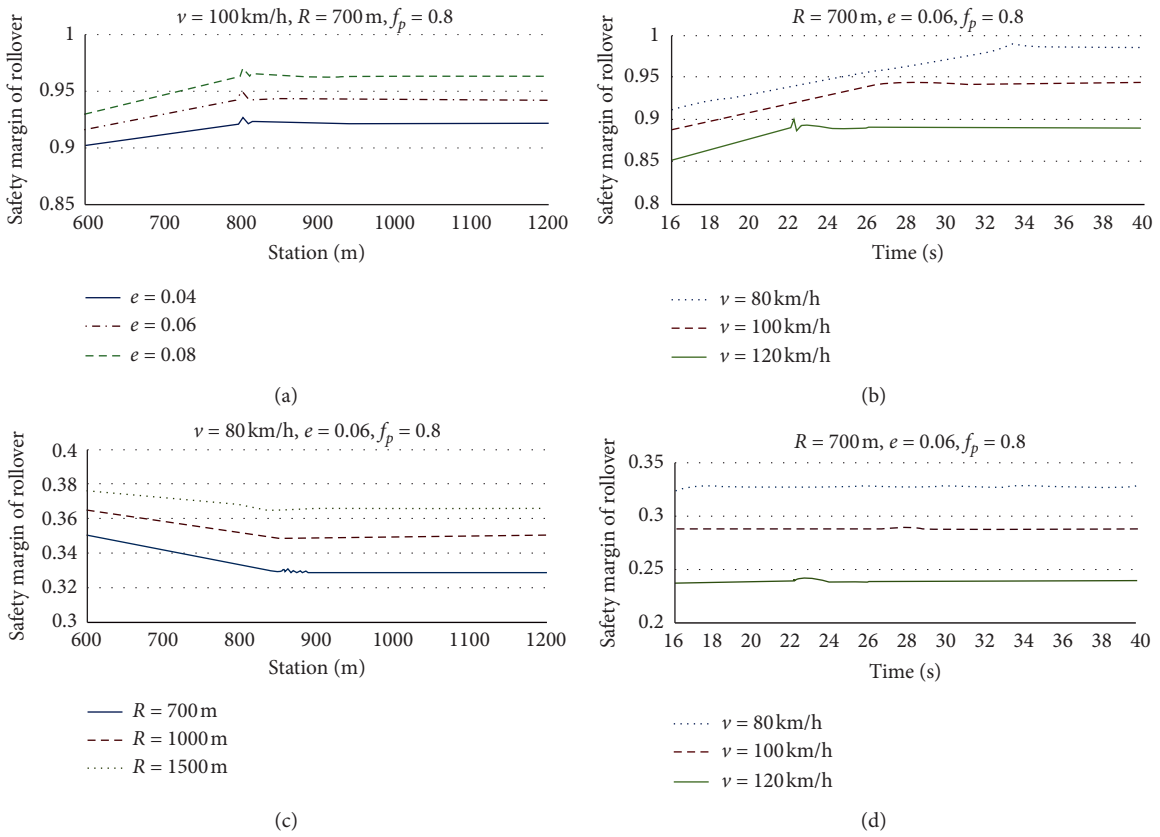

Figure 8: The effect of the significant single factor on the safety margin of vehicle rollover. (a) Effect of superelevation on the safety margin of rollover. (b) Effect of speed on the safety margin rollover. (c) Effect of the radius of the horizontal curve on the safety margin of rollover (M_3). (d) Effect of speed on the safety margin of rollover (M_3).

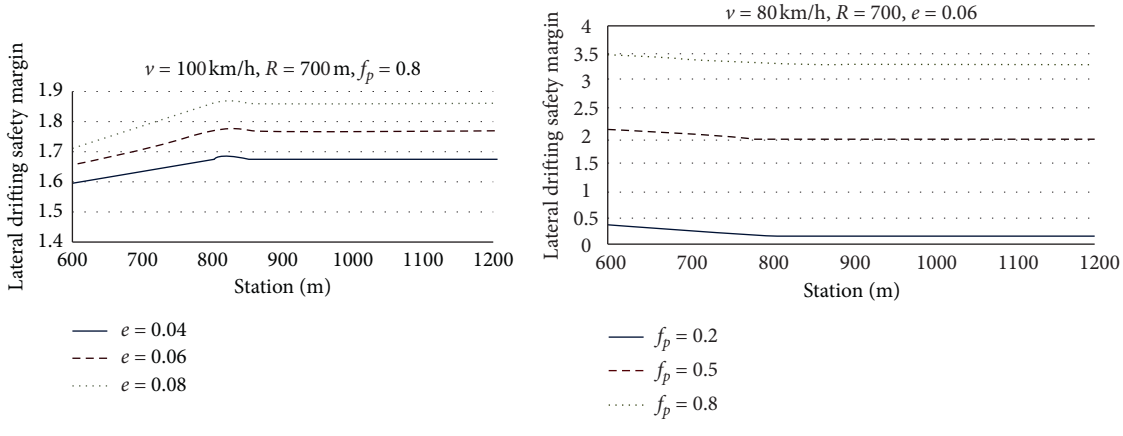

Figure 9: Continued.

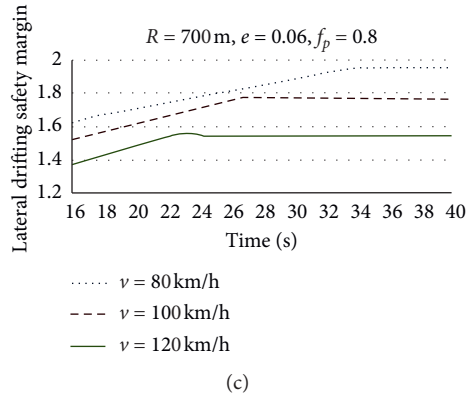

Figure 9: The effect of the significant single factor on the safety margin of the vehicle's lateral drift. (a) Effect of superelevation on the safety margin of lateral drifting. (b) Effect of the peak friction coefficient on the safety margin of lateral drifting. (c) Effect of speed on the safety margin of lateral drifting.

is a circular curve section. The values of superelevation are $e = 0.04, 0.06, 0.08$. As can be seen from Figure 9(a), with the increase in superelevation, the safety margin of the vehicle's lateral drift increases. Therefore, vehicles are less prone to lateral drift.

Figure 9(b) shows the effect of the maximum tire-road friction coefficient on the safety margin of lateral drift. The speed $v = 80$ (km/h), radius of the circular curve $R = 700$ m, and the superelevation $e = 0.06$. The 600 m–1200 m road section is selected as the research object. The 600–800 m road section is the transition section from a straight line to a circular curve (clothoid curve section). The 800–1200 m road section is a circular curve section. The maximum tire-road friction coefficients are $f_p = 0.2, 0.5, 0.8$. As can be seen from Figure 9(b), with the increase in the maximum tire-road friction coefficient, the safety margin of lateral drift increases. Therefore, it is more difficult for the vehicle to drift.

Figure 9(c) shows the effect of vehicle speed on the safety margin of the vehicle's lateral drift. Radius of the circular curve $R = 700$ m, the superelevation $e = 0.06$, and the maximum tire-road friction coefficient $f_p = 0.8$. The road section of time at 16 s–40 s is selected as the research object, which includes two sections: the transition section (clothoid curve section) and circular curve section. The vehicle speeds are $v = 80$ (km/h), 100 (km/h), 120 (km/h). As can be seen from the Figure 9(c), with the increase in vehicle speed, the safety margin of the vehicle's lateral drift reduces. Therefore, vehicles are more prone to lateral drift.

5. Conclusions

Based on the analysis of vehicles accident in a curve, the skidding, rollover, and lateral drift of vehicles are determined as the means to evaluate the lateral stability of vehicles. Aiming at the high accident rate of utility trucks with rear-wheel drive (RWD), simulation models of Human-Vehicle-Road are established by CarSim. Through the orthogonal analysis design method, the effects of road geometry, speed factors, and interaction between road geometries on the lateral stability of vehicles are studied.

In this paper, the lateral force coefficient is used to characterize the safety margin of vehicle skidding. Synthesizing the results of orthogonal analysis and range analysis of the safety margin of vehicle skidding, it is suggested that the maximum tire-road friction coefficient and vehicle speed have a highly significant effect on vehicle skidding. The superelevation has a significant influence on vehicle's skidding. The interaction of horizontal alignment and superelevation has an important effect on vehicle skidding. It cannot be ignored.

Significant single factor analysis shows that, with the increase of superelevation and the maximum tire-road friction coefficient, the safety margin of vehicle skidding increases, and the vehicle is less prone to skidding. With the increase of vehicle speed, the safety margin of vehicle skidding decreases, and the vehicle is more prone to skid.

In this paper, lateral acceleration and the load transfer ratio are used to characterize the safety margin of vehicle rollover. The results of orthogonal analysis and range analysis show that horizontal alignment and vehicle speed have a highly significant impact on vehicle rollover risk. The superelevation has a significant impact on vehicle rollover risk, and the interaction between horizontal alignment and superelevation is also an important factor.

Significant single factor analysis shows that, with the increase of superelevation and the radius of horizontal curves, the safety margin of vehicle rollover increases, and the rollover of vehicles is less prone to occur. With the increase of vehicle speed, the safety margin (M_2, M_3) of vehicle rollover decreases, and the vehicle is more prone to rollover.

In this paper, the safety margin of the vehicle's lateral drift is characterized by the sideslip angle. From the results of orthogonal analysis and range analysis, we can get these conclusions. The vehicle speed and maximum tire-road friction coefficient have a highly significant effect on the vehicle's lateral drift. The superelevation has a significant effect on the vehicle's lateral drift. The interaction of horizontal alignment and superelevation and longitudinal slope has an important effect on the vehicle's lateral drift. It cannot be ignored.

Significant single factor analysis shows that, with the increase in superelevation, the safety margin of vehicles' lateral drift increases, and the lateral drift of vehicles is less likely to occur. With the increase in vehicle speed and the maximum tire-road friction coefficient, the safety margin of the vehicle's lateral drift decreases, and the lateral drift of vehicles is more likely to occur.

The results of the abovementioned analysis show that the vehicle traveling risk can be reduced through improving and limiting the significant adverse factors for the lateral stability of vehicles. In our future research, besides considering the influence of a single factor on vehicle lateral stability, we should also consider the interaction among multiple factors.

Data Availability

Some or all data, models, or code generated or used during the study are available in a repository or online in accordance with funder data retention policies (provide full citations that include URLs or DOIs).

Conflicts of Interest

The authors declare no conflicts of interest.

Authors' Contributions

L. S. conceived the study; Y. Y. and L. S. conducted the numerical experimental design; Y. Y., H. W., and L. S. analyzed the data and wrote the paper; and W. H. participated in the revision of the study and providing suggestions on incorporation of technical specifications of road geometric design and policy recommendations.

Acknowledgments

This study was sponsored in part by the National Natural Science Foundation of China under grants 51050110143 and 51250110075 and by Qilu Transportation Development Group, to which the authors are very grateful.

Supplementary Materials

This form can be seen in the supplementary document (Experimental data). The supplementary document is the selected orthogonal table and the experimental data for orthogonal analysis. (*Supplementary Materials*)

References

[1] NHTSA, National Highway Traffic Safety Administration, 2016, http://www.nhtsa.dot.gov.

[2] D. Chu, Z. Li, J. Wang, C. Wu, and Z. Hu, "Rollover speed prediction on curves for heavy vehicles using mobile smartphone," *Measurement*, vol. 130, pp. 404–411, 2018.

[3] S. Yim, "Design of a robust controller for rollover prevention with active suspension and differential braking," *Journal of Mechanical Science and Technology*, vol. 26, no. 1, pp. 213–222, 2012.

[4] S. Yim, K. Jeon, and K. Yi, "An investigation into vehicle rollover prevention by coordinated control of active anti-roll bar and electronic stability program," *International Journal of Control, Automation and Systems*, vol. 10, no. 2, pp. 275–287, 2012.

[5] A. B. Dunwoody and S. Froese, "Active roll control of a semi-trailer," SAE International, Warrendale, PA, USA, SAE Technical Paper 933045, 1993.

[6] J. Shin and I. Lee, "Reliability-based vehicle safety assessment and design optimization of roadway radius and speed limit in windy environments," *Journal of Mechanical Design*, vol. 136, no. 8, Article ID 081006, 2014.

[7] T. Sayed, W. Abdelwahab, and F. Navin, "Identifying accident-prone locations using fuzzy pattern recognition," *Journal of Transportation Engineering*, vol. 121, no. 4, pp. 352–358, 1995.

[8] K. Rumar, "The Role of Perceptual and Cognitive Filters in Observed Behavior," *Human Behavior and Traffic Safety*, Springer, Boston, MA, USA, pp. 151–170, 1985.

[9] J. Shin and I. Lee, "Reliability analysis and reliability-based design optimization of roadway horizontal curves using a first-order reliability method," *Engineering Optimization*, vol. 47, no. 5, pp. 622–641, 2015.

[10] F. Malin, I. Norros, and S. Innamaa, "Accident risk of road and weather conditions on different road types," *Accident Analysis & Prevention*, vol. 122, pp. 181–188, 2019.

[11] S. Mavromatis and B. Psarianos, "Analytical model to determine the influence of horizontal alignment of two-axle heavy vehicles on upgrades," *Journal of Transportation Engineering*, vol. 129, no. 6, pp. 583–589, 2003.

[12] S. Mavromatis, F. Mertzanis, G. Kleioutis et al., "Three-dimensional stopping sight distance control on passing lanes of divided highways," *European Transport Research Review*, vol. 8, no. 1, p. 8, 2016.

[13] S. Mavromatis, A. Laiou, and G. Yannis, "Safety assessment of control design parameters through vehicle dynamics model," *Accident Analysis & Prevention*, vol. 125, pp. 330–335, 2019.

[14] K. S. You, L. Sun, and W. J. Gu, "Risk analysis-based identification of road hazard locations using vehicle dynamic simulation," *Journal of Southeast University (Natural Science Edition)*, vol. 42, no. 1, pp. 151–155, 2012.

[15] K. S. You, L. Sun, and W. J. Gu, "Reliability design theory and method of highway horizontal curve radius," *Journal of Traffic and Transportation Engineering*, vol. 12, no. 6, pp. 1–6, 2012.

[16] K. You and L. Sun, "Reliability analysis of vehicle stability on combined horizontal and vertical alignments: driving safety perspective," *Journal of Transportation Engineering*, vol. 139, no. 8, pp. 804–813, 2013.

[17] Y. Liu, R. You, and Y. Yang, *Road Reconnaissance Design (In Chinese)*, China Electric Power Press, Beijing, China, 2010.

[18] M. Kontaratos, B. Psarianos, and A. Yiotis, "Minimum horizontal curve radius as a function of grade incurred by vehicle motion in driving mode," *Journal Transportation Research Record*, vol. 1445, pp. 86–93, 1994.

[19] H. B. Pacejka, *Tire and Vehicle Dynamics, Society of Automotive Engineers*, Butterworth – Heinemann, London, UK, 2006.

[20] K. S. You, *Vehicle Dynamic and Reliability Reliability Based Highway Safety Analysis and Design Optimization*, Southeast University, Nanjing, China, 2012.

[21] W. Zhang, *Vehicle Dynamics Analysis of Single Vehicle Road Traffic Accident and Regression Model*, Xiamen University, Xiamen, China, 2017.

[22] Mechanical Simulation Corporation, *CARSIM Reference Manual*, Mechanical Simulation Corporation, Ann Arbor, MI, USA, 2016.
[23] E. Bakker, L. Nyborg, and H. B. Pacejka, "Tyre modelling for use in vehicle dynamics studies," pp. 190–192, SAE International, Warrendale, PA, USA, 1987, SAE Technical Paper Series.
[24] E. Bakker, H. B. Pacejka, and L. Lidner, "A new tire model with an application in vehicles dynamics studies," pp. 101–113, SAE International, Warrendale, PA, USA, 1989, SAE Paper 890087.
[25] F. Yu and Y. Lin, *Automotive System Dynamics*, China Machine Press, Beijing, China, 2016.
[26] L. Sun, K. S. You, Y. Wang et al., "Influence analysis of road conditions on vehicle rollover," *Journal of Southeast University (Natural Science Edition)*, vol. 43, no. 3, pp. 645–648, 2013.
[27] D. Wang, L. He, X. J. Sun et al., "Parameters identification of magic formula of vehicle tire using genetic algorithm," *Bus & Coach Technology and Research*, vol. 2, 2015.
[28] C. Zhang, L. Meng, and S. J. Wang, "Sideslip risk simulation analysis of passenger car braking behavior on expressway curved sections," *China Journal of Highway and Transport*, vol. 28, no. 12, pp. 134–142, 2015.
[29] C. C. Macadam, "Application of an optimal preview control for simulation of closed-loop automobile driving," *IEEE Transactions on Systems, Man, and Cybernetics*, vol. 11, 1981.
[30] C. C. Macadam, "An optimal preview control for linear systems," *Journal of Dynamic Systems, Measurement, and Control, ASME*, vol. 102, no. 3, 1980.
[31] M. Abe, *Vehicle Handling Dynamics Theory and Application*, China Machine Press, Beijing, China, 2016.
[32] Z. S. Yu, *Automobile Theory*, China Machine Press, Beijing, China, 2011.
[33] R. Lamm, B. Psarianos, and T. Mailaender, *Highway Design and Traffic Safety Engineering Handbook*, McGraw-Hill Companies, New York, NY, USA, 1999.
[34] S. Dieter, H. Manfred, and B. Roberto, *Vehicle Dynamics: Modeling and Simulation*, Springer-Verlag Berlin Heidelberg, Berlin, Germany, 2018.
[35] D. W. Harwood and J. M. Mason, *Horizontal Curve Design for Passenger Cars and Trucks*, pp. 22–33, Transportation Research Board, Washington, DC, USA, 1994.
[36] Z. C. Su, *Study on Vehicle Dynamic Stability Control on Steering and Braking Maneuvers*, Chongqing University, Chongqing, China, 2007.
[37] F. Zhang, J. Gonzales, K. Li et al., "Autonomous drift cornering with mixed open-loop and closed-loop control," *IFAC Papers On Line*, vol. 50, pp. 1916–1922, 2017.
[38] E. Velenis, "FWD vehicle drifting control: the handbrake-cornering technique," in *Proceedings of the 2011 50th IEEE Conference on Decision and Control and European Control Conference (CDC-ECC)*, pp. 3258–3263, Orlando, FL, USA, December 2011.
[39] R. Y. Hindiyeh and J. C. Gerdes, "Design of a dynamic surface controller for vehicle sideslip angle during autonomous drifting," in *Proceedings of the 6th IFAC Symposium Advances in Automotive Control Munich*, Munich, Germany, July 2010.
[40] C. Q. Zhang and C. X. He, *Fundamentals of Mathematical Statistics*, South China University of Technology Press, Guangzhou, China, 2013.